Journal of Power Sources 222 (2013) 442–447

Contents lists available at SciVerse ScienceDirect

Journal of Power Sources

journal homepage: www.elsevier.com/locate/jpowsour

Electrochemical impedance spectroscopy analysis for lithium-ion battery using $Li_4Ti_5O_{12}$ anode

Tao Hang [a], Daikichi Mukoyama [a], Hiroki Nara [a], Norio Takami [b], Toshiyuki Momma [c,*], Tetsuya Osaka [c,*]

[a] Research Institute for Science and Engineering, Waseda University, 3-4-1 Okubo, Shinjuku, Tokyo 169-8555, Japan
[b] Corporative Research & Development Center, Toshiba Corporation, Saiwai-ku, Kawasaki 212-8582, Japan
[c] Department of Applied Chemistry, School of Advanced Science and Engineering, Faculty of Science and Engineering, Waseda University, 3-4-1 Okubo, Shinjuku, Tokyo 169-8555, Japan

HIGHLIGHTS

- The impedance of LIB with LTO anode was interpreted by a proposed equivalent circuit.
- The cathode with two sets of different parameters was considered.
- The fitting results at different SOC or temperature are consistent with previous report.
- The capacity fade due to cycling is mainly caused by degradation of the cathode.
- The cyclability of this LIB was improved by using a LTO anode instead of graphite anode.

GRAPHICAL ABSTRACT

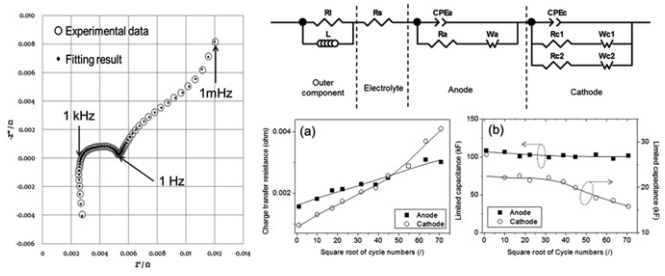

ARTICLE INFO

Article history:
Received 24 July 2012
Received in revised form
31 August 2012
Accepted 3 September 2012
Available online 10 September 2012

Keywords:
Li-ion battery
Electrochemical impedance spectroscopy
$Li_4Ti_5O_{12}$ anodes
Capacity fade

ABSTRACT

The impedance of Li-ion battery using a $Li_4Ti_5O_{12}$ (LTO) anode for high-power applications was measured at various depths of discharge and temperatures during charge–discharge cycles. The measured impedance was interpreted with an equivalent circuit made up of anode and cathode, in which the cathode component was composed of two particle size factors. The values obtained for equivalent circuit elements by modeling were in good agreement with the results measured by other techniques, and indicated that the capacity fade of this Li-ion battery due to cycling is mainly caused by the increase of interfacial resistance and a decrease in the capacity of the $LiCoO_2$ cathode. These results suggest that the cyclability of this LIB was improved by using an LTO anode, and show the validity of the equivalent circuit for interpreting the causes of capacity fade.

1. Introduction

In order to succeed in future large-scale applications such as hybrid electric vehicles (HEVs), Li-ion batteries (LIBs) need to achieve a high-power density, an excellent cycle-life, low-temperature performance, light weight, and meet reliability and safety requirements [1]. Since safety and life limitations of LIBs are the most important subjects with regard to commercialization of high-power lithium-ion batteries, the techniques to evaluate the cycling behavior and stability will be of significant importance.

Many efforts have been made by various groups to study the mechanism of the capacity fading of LIBs [2,3]. However, to

* Corresponding authors. Tel.: +81 3 5286 3202; fax: +81 3 3205 2074.
E-mail addresses: momma@waseda.jp (T. Momma), osakatets@waseda.jp (T. Osaka).

0378-7753/$ – see front matter © 2012 Elsevier B.V. All rights reserved.
http://dx.doi.org/10.1016/j.jpowsour.2012.09.010

understand the complex electrochemical reaction for commercial batteries, the battery cell usually needs to be disassembled, which is inconvenient and does not allow for tracking of the continuous changes with cycling.

Electrochemical impedance spectroscopy (EIS) is a very helpful technique for separating the electrochemical reactions and evaluating each parameter quantitatively without opening the battery cell [4]. Previous studies have shown that measured impedance spectra consisted of a small semicircle at high frequency, a large semicircle at middle frequency, and a diffusion related impedance response at low frequency. The measurements performed with and without a reference electrode showed that the small semicircle at high frequency was mainly attributed to the anode while the large one at mid-frequency was attributed to the cathode. The influences of the battery temperatures and charge–discharge cycles were also studied by analyzing mainly the two semi-circles on the impedance spectra [5–7]. However, few studies were concerned about the impedance of lithium diffusion at low frequency.

Previously, our group proposed an equivalent circuit for commercial Li-ion batteries for a wide range of impedance spectra [8,9]. The impedances of prismatic commercial batteries were measured without reference electrodes, and the fitting results showed that this was a convenient method to study the capacity fade with two-electrode measurements [8,10].

In this work, the equivalent circuit was applied to a Li-ion battery sample with a combination of lithium titanate spinel $Li_4Ti_5O_{12}$ (LTO) anode and $LiCoO_2$ (LCO) cathode. The most attractive characteristics of LTO are its very flat discharge–charge plateau at 1.5 V and its excellent cycle-life [11–13]. This material can accommodate lithium ions during the charging process, resulting in a structural transition from spinel to rock-salt phase without a noticeable change in lattice parameter. Intensive studies have demonstrated that this so-called “zero-strain material” offers excellent cycle-life without capacity fade after hundreds of cycles [14–17]. Moreover, LTO may not form a solid electrolyte interface (SEI) and can operate well with propylene carbonate solvent without the risk of exfoliation[18]. These features could make a cell based on LTO spinel to operate safely at both low and high temperatures [19].

Up to now, only few EIS studies on the characterization of the electrochemical properties of LTO exist, in which the impedance behavior of LTO at several state-of-charge (SOC) values is reported [20,21]. In addition, the effect of different amounts of active material on the frequency response was investigated [22].

Here, in contrast to already existing work, new insights into the impedance behavior of LTO/LCO battery sample were gained by performing measurements at different temperatures as well as during several thousand cycles. The state of the batteries was analyzed to demonstrate how the capacity fade of commercial batteries can be assessed in a nondestructive method.

2. Experimental details

Li-ion battery samples were 4 Ah-class batteries using the $Li_4Ti_5O_{12}$ anode and the $LiCoO_2$ cathode for high-power applications. The batteries were charged and discharged with a constant current (CC) protocol between 1.8 and 2.8 V with a rate of 4 C at room temperature. The impedance of the batteries was measured by a potentiostat (Solartron, 1400) and a frequency response analyzer (Solartron, 1400) with AC signal amplitude of 5 mV in the frequency range from 100 kHz to 1 mHz. During the impedance measurement, the batteries were charged at a rate of 1.0 C to 2.8 V, and were maintained at 2.8 V for 3 h (depth of discharge (DOD) = 0%), then discharged at a rate of 1.0 C. During the discharge, the current was stopped to obtain LIBs with different DODs. Another set of batteries was measured at temperatures of −20 °C, 0 °C, 25 °C, 40 °C and 60 °C.

Data fitting was carried out with Microsoft Excel Solver to reach the minimum value of the total error, i.e., the sum of the difference between the acquired experimental complex impedance data and the impedances calculated with the equivalent circuit using the parameters obtained by fitting for each frequency.

3. Results and discussion

3.1. Equivalent circuit and typical fitting parameter

Measured impedances were fitted with the equivalent circuit shown in Fig. 1. The descriptions of this circuit are written in detail elsewhere [8]. In short, the circuit was designed with a basic idea of variation in diffusion length of Li^+ in the active material in the cathode. For simplicity, two typical diffusion elements were considered to represent a model having two types of active materials with two different radii. Two sets of series connection of diffusion element and charge transfer resistance are connected in parallel, with an element representing the capacitance between the electrolyte and the particles. The variation of the capacitance in particles is represented by a constant phase element (CPE) [23]. The capacitors for the particles with both radii are connected in parallel and simplified as one CPE.

The two Warburg (diffusion) impedances in parallel can be expressed by:

$$Z_D = \sigma(1-j)\omega^{-(1/2)}\mathrm{Coth}\left(L\sqrt{\frac{j\omega}{D}}\right) \quad (1)$$

$$\sigma = \frac{L}{\sqrt{2DC_L}} \quad (2)$$

where ω is frequency, L is the diffusion length, D is the diffusion coefficient, σ is the diffusion constant, and C_L is the limiting capacitance[24].

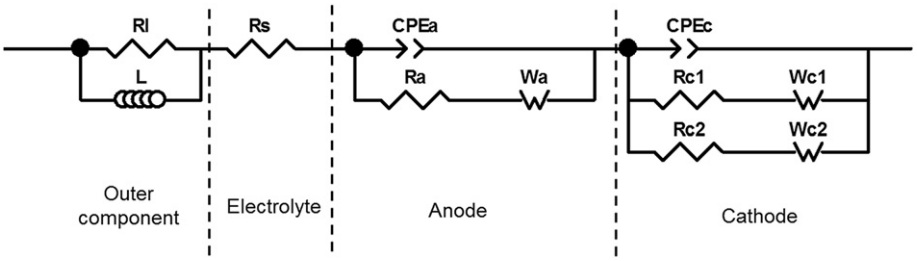

Fig. 1. Equivalent circuit for impedance analysis in this study. Symbols of the equivalent circuit were expressed as follows: L, inductance of current collector and battery case; R_l, resistance of current collector; R_s, resistance of electrolyte and current collector; R_a, R_{c1} and R_{c2}, interfacial charge transfer resistance; CPE_a and CPE_c, capacitance of electrode surface layer; W_a, W_{c1} and W_{c2}, Warburg impedance.

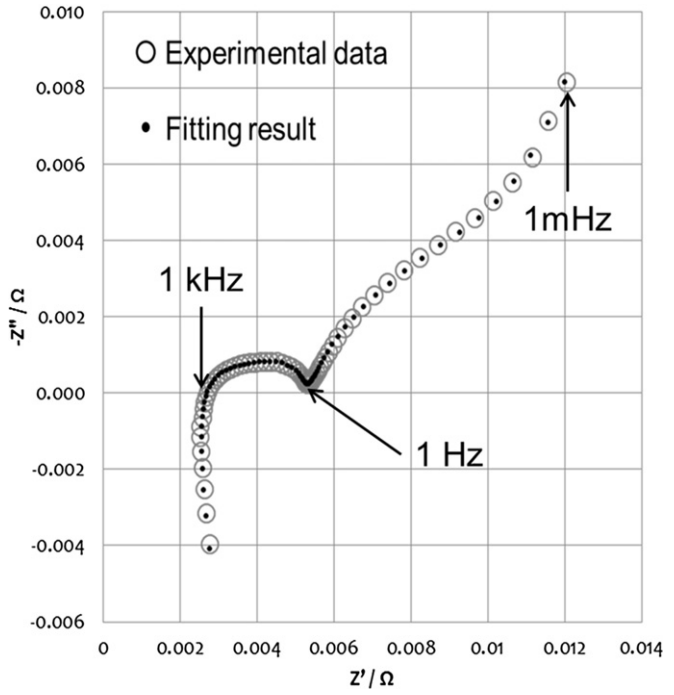

Fig. 2. Typical fitting plots of experimental impedance spectrum of 4 Ah-class LTO/LCO battery sample measured at DOD 20%, 25 °C, frequency range: 10 kHz–1 mHz, signal amplitude 5 mV.

It is reported that the LTO anodes do not develop surface films as other Li insertion electrodes, which operate at low potentials (such as Li-carbon electrodes) or at high potentials (such as many lithiated transition metal oxides) [18,25]. Thus in this study, the component of solid–electrolyte interphase (SEI) was not taken into consideration. This is different from our previously proposed equivalent circuit for LIB with a carbon anode [9].

Typical fitting plots of this LTO/LCO battery sample are illustrated with the data of the ac impedance responses in Fig. 2. The dotted curve shows the impedance calculated using the equivalent circuit. The error between the experimental and calculated data was small. The typical fitting parameters for the impedance at 20% DOD obtained with the equivalent circuit, are shown in Table 1.

3.2. Impedance depending on the depths of discharge

The impedances of the batteries with various depths of discharge (DODs) were measured and fitted to the equivalent circuit shown in Fig. 1. The fitted values of resistance are shown in Fig. 3a. It is suggested that the charge transfer resistance of the cathode (R_c), which was calculated as parallel connection of R_{c1} and R_{c2}, increased from 1 mΩ to 2.4 mΩ with the increase of DOD from 10% to 90%. This result is close to the previous report on charge transfer resistance for the LCO cathode of commercial lithium battery [8]. The charge transfer resistance of the anode (R_a) was nearly constant for the DOD ranges used here, which also shows a similar behavior to the reported LTO anode in all-solid-state LIB [22]. However, the fitted value of R_s shows a slight increase with the increase of DOD. This phenomenon might be attributed to the significant change of electronic conductivity of LTO during discharge. The component of R_s in the equivalent circuit may include resistances which are connected potentially in series, such as the electronic resistances of current collector and electrode, as well as the ionic resistance of electrolyte. Since the electronic conductivity of LTO significant changed with the state-of-charge [26], the resistance change of LTO might affect the value of R_s.

In the assumption that the diffusion lengths (L) are equal to the radii of the particles of electrode materials and keep constant at different DODs, the Li-ion diffusion coefficients (D) in both electrodes can be obtained from the fitted values of L^2/D, which are shown in Fig. 3(b). The plot shows that the D value of the cathode decreased from ca. 10^{-9} to 10^{-10} cm^2 s^{-1}, and that of anode increased from ca. 10^{-12} to 10^{-11} cm^2 s^{-1} with the increase of DOD

Table 1
Typical fitting parameters.

Outer component	R_0	0.521 Ω
	L_0	0.0435 μH
Electrolyte	R_s	2.39 mΩ
Anode	R_a	1.64 mΩ
	CPE_a-T	3.97
	CPE_a-p	0.724
	D of W_a	1.33×10^{-12} cm^2 s^{-1}
	L of W_a	0.5 μm (fixed)
	C_L of W_a	56.5 kF
Cathode	R_{c1+c2}	0.982 mΩ
	CPE_c-T	9.37
	CPE_c-p	1.00
	D of W_c	9.11×10^{-10} cm^2 s^{-1}
	L of W_{c1}	5 μm (fixed)
	C_L of W_{c1}	27.7 kF
	L of W_{c2}	0.1 μm (fixed)
	C_L of W_{c2}	1.93 kF

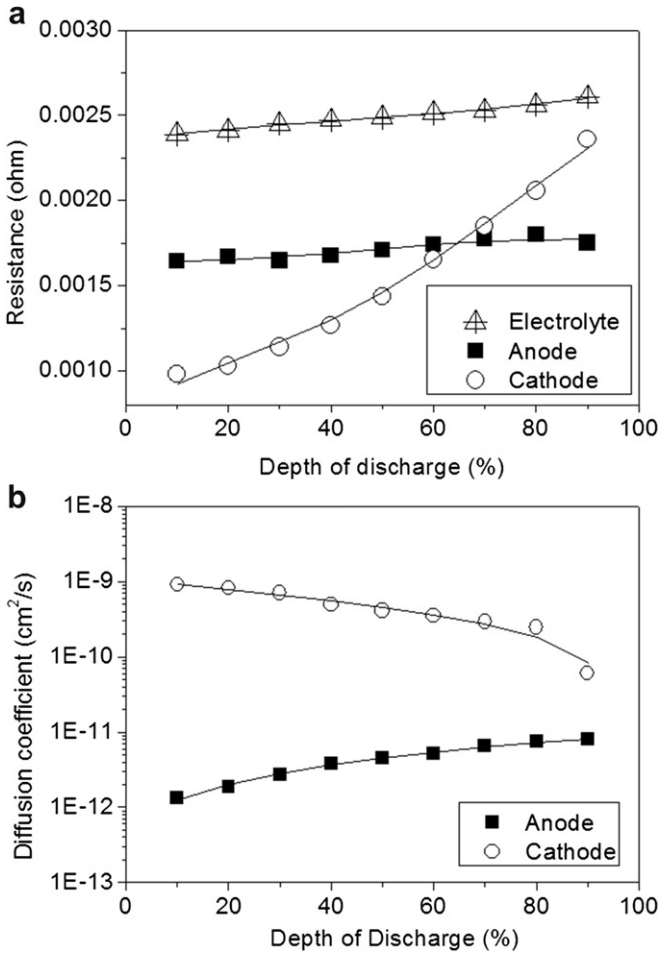

Fig. 3. Plots of the values obtained from the fits of the impedance at different depths of discharge: (a) electrode–electrolyte interface resistance; (b) diffusion coefficient in Warburg impedance.

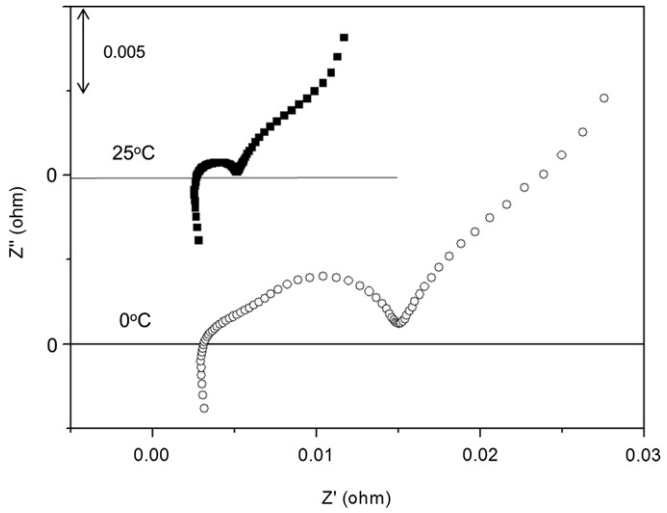

Fig. 4. Impedance spectra for lower (0 °C) and higher (25 °C) temperatures at 20% DOD.

from 10% to 90%. These results for Li-ion diffusion coefficients are consistent with previous results on lithium diffusion in LTO anode [27] and other reports on LCO cathode [28,29].

3.3. Impedance at different temperatures

The influence of temperature was investigated at five points between −20 °C and 60 °C. The temperature influence on the impedance spectrum is strong, as expected. Since the spectra ranges differ extremely with temperature, we only show the impedance spectra measured at 0 °C and 25 °C in Fig. 4 for comparison. At lower temperatures (below 0 °C), a spread of both semi-circles can be observed. This spread is a consequence of slower chemical processes at low cell temperatures and corresponding higher cell impedance. For higher temperatures (above 25 °C) both semi-circles grow together and cannot be distinguished, indicating the time constants of the internal processes become similar, and a separation is not possible anymore. A similar trend has been reported for other LIB in previous reports [7,30].

Fig. 5 shows the dependence of resistance on inverse temperature at the DOD of 50%. The apparent activation energies (E_a) for the electrochemical reactions corresponding to R_a and R_c were calculated from the gradients of the Arrhenius plots in Fig. 5. The E_a of R_a was ca. 29 kJ mol^{-1}, and that of R_c was ca. 58 kJ mol^{-1}. The values of E_a are almost constant in the wide DOD range. The E_a of R_c is also consistent according to the data that has already been reported for LTO anode [31] and LCO cathode [32,33], which further supports the efficacy of the model in assignment of values for each components.

3.4. Impedance of charge–discharge cycles

During continuous charge–discharge cycling of the LIBs, it was observed that the discharging capacity linearly faded with the cycling, as shown in Fig. 6. The initial capacity at the DOD of 0% is more than 4.4 Ah, and it gradually decreases to less than 3.9 Ah after 5000 charge–discharge cycles at a rate of 4.0 C. The capacity was found to decrease as a linear function of the square root of the cycle numbers before 1500 cycles. The mechanism thought to be responsible for this capacity fade is the growth of a surface film on the anode and/or cathode as the battery cycles [34,35]. It can also be seen that after about 1500 cycles, the capacity begins to decrease faster. The reason for this sudden increase in the capacity fade rate is unknown so far.

The measured impedance was fitted to the equivalent circuit used above. The fitted values of charge transfer resistances are plotted in Fig. 7(a), showing that the charge transfer resistance of both anode and cathode increased with the cycle numbers, although the interfacial resistance of the cathode increased much faster than that of the anode. Furthermore, the resistance increase rate of the cathode was accelerated after 1500 cycles, which is consistent with the capacity fade behavior. These results could be interpreted as showing that the surface layer on the anode is growing slowly during cycling, and the surface layer on the cathode grows faster due to the strong oxidizing power of Co^{4+} in the charged state [5].

The values of limiting capacitance obtained from fitting are shown in Fig. 7(b). The capacitance of the LCO cathode decreased from 27.1 kF to 22.1 kF during the first 100 cycles which could be attributed to the formation of the surface film resulting in a decrease of the active sites. After that, the capacitance of LCO cathode kept constant for about 1000 cycles but started to decrease after 1500 cycles. The decrease of long term cycling

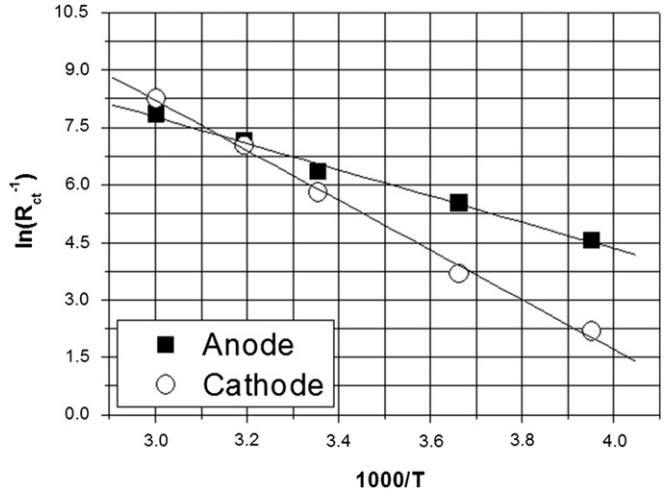

Fig. 5. Arrhenius plot for the electrochemical reactions corresponding to charge transfer resistance of anode and cathode at DOD of 20%.

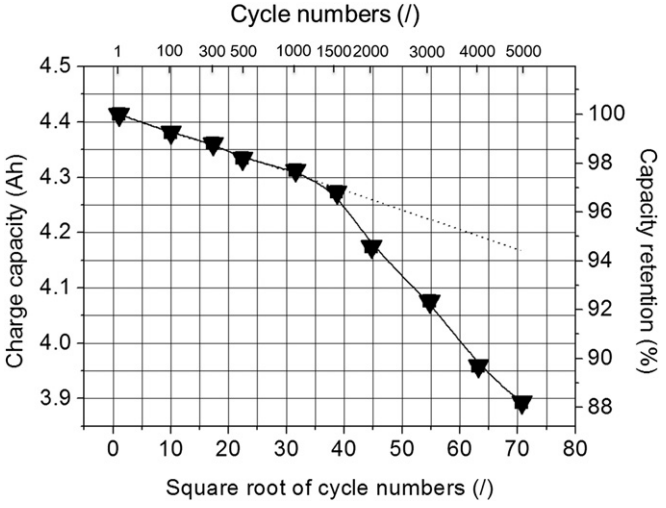

Fig. 6. Battery charge capacity with the number of charge–discharge cycles.

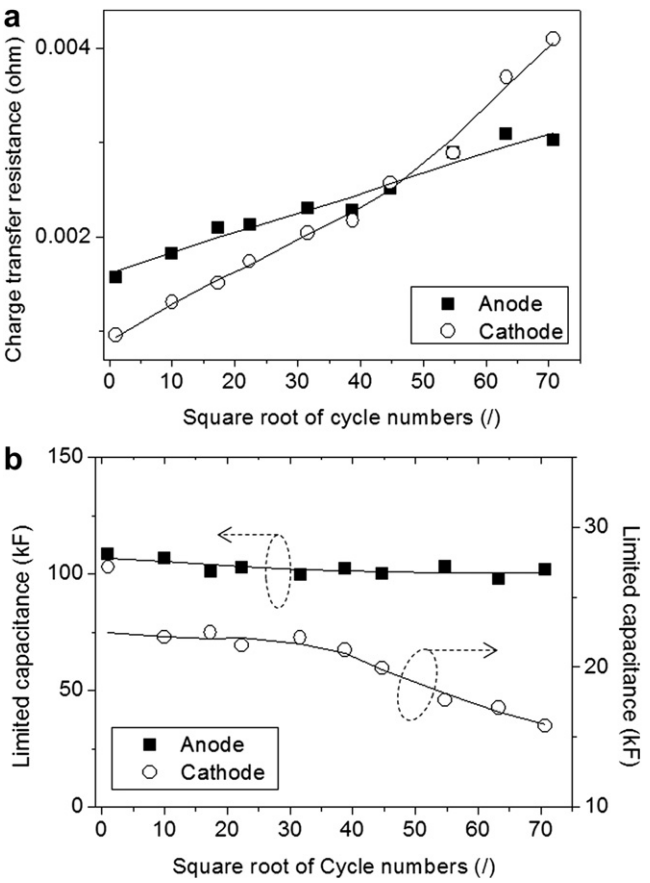

Fig. 7. Variation of the (a) resistance and (b) limiting capacity with the number of charge–discharge cycles at DOD of 20%.

might be due to complete disconnection of some particles, removing them from the process of charge storage. The capacitance of the LTO anode is one order larger than that of the cathode and remains almost constant during 5000 cycles. The limiting capacitance of the cathode is remarkably low compared with that of the anode. In LIBs, electrodes are aligned in series along the direction of current, and the lowest capacitance should be the dominant. Therefore, the total limiting capacitance is regulated by the decrease in the limiting capacitance of the cathode with an increase in the number of cycles. Hence, the cell degradation was mainly attributed to both the resistance increase and the capacity decrease of cathode. The mechanism could be explained as following. Before 1500 cycles, the formation and growth of the surface film on cathode dominated the capacity fade. But after 1500 cycles, the reaction sites of the cathode material as well as the diffusion path for lithium ion started to decrease, which resulted in an accelerated increase of the interfacial resistance and a decrease of the limiting capacity. These results suggest that the cycle stability of the LTO anode is better than that of the LCO cathode. Moreover, compared to the conventional LIB studied in our previous work, for which the capacity fading was attributed to the capacity decrease of the carbon anode, the LTO/LCO battery exhibits an excellent cycling performance by using the LTO anode. The analysis with the proposed equivalent circuit enables interpretation of the battery impedance behavior measured with the two-electrode system for a wide range of frequencies on various commercial LIBs, and provides a proper analysis method for the study of capacity fading.

4. Conclusions

The impedance of Li-ion battery samples using the LCO cathode and the LTO anode were measured under various conditions. The impedance was fitted with a previously proposed equivalent circuit. The plots of the fitted values versus depth of discharge showed similar trends to those observed by other groups. Thus, the fitting parameters can be assigned to each electrode in the comparison. With the assignments, the impedance of the battery after cycling was analyzed, showing that the capacity fade was mainly caused by an interfacial resistance increase and a capacity decrease of the cathode. These results suggested that the cycling performance of the LTO anode is better than that of the conventional carbon anode in our previous study, and demonstrated that two-electrode measurements of battery impedance for a wide range of frequencies can be interpreted with the equivalent circuit, providing an analysis tool for the study of electrochemical properties of various commercial LIB.

Acknowledgments

This work was supported by “Research & Development Initiative for Scientific Innovation of New Generation Batteries” from the New Energy and Industrial technology Development Organization of Japan and a Grant-in-Aid for Specially Promoted Research “Establishment of Electrochemical Device Engineering” from the Ministry of Education, Culture, Sports, Science and Technology, Japan and done in the Center for Practical Chemical Wisdom of Global COE.

References

[1] N. Takami, H. Inagaki, T. Kishi, Y. Harada, Y. Fujita, K. Hoshina, Journal of the Electrochemical Society 156 (2009) A128–A132.
[2] P. Arora, R.E. White, M. Doyle, Journal of the Electrochemical Society 145 (1998) 3647–3667.
[3] J.S. Kim, Y.T. Park, Journal of Power Sources 91 (2000) 172–176.
[4] T. Kobayashi, S. Seki, Y. Mita, H. Miyashiro, N. Terada, T. Kojima, Electrochemistry 78 (2010) 416–419.
[5] D. Zhang, B.S. Haran, A. Durairajan, R.E. White, Y. Podrazhansky, B.N. Popov, Journal of Power Sources 91 (2000) 122–129.
[6] G. Nagasubramanian, Journal of Power Sources 87 (2000) 226–229.
[7] T. Momma, M. Matsunaga, D. Mukoyama, T. Osaka, Journal of Power Sources 216 (2012) 304–307.
[8] T. Osaka, S. Nakade, M. Rajamaki, T. Momma, Journal of Power Sources 119 (2003) 929–933.
[9] T. Osaka, T. Momma, D. Mukoyama, H. Nara, Journal of Power Sources 205 (2012) 483–486.
[10] D. Mukoyama, T. Momma, H. Nara, T. Osaka, Chemistry Letters 41 (2012) 444–446.
[11] T. Ohzuku, A. Ueda, N. Yamamoto, Y. Iwakoshi, Journal of Power Sources 54 (1995) 99–102.
[12] T. Ohzuku, A. Ueda, N. Yamamoto, Journal of the Electrochemical Society 142 (1995) 1431–1435.
[13] J.X. Ma, C.S. Wang, S. Wroblewski, Journal of Power Sources 164 (2007) 849–856.
[14] C.H. Chen, J.T. Vaughey, A.N. Jansen, D.W. Dees, A.J. Kahaian, T. Goacher, M.M. Thackeray, Journal of the Electrochemical Society 148 (2001) A102–A104.
[15] M. Venkateswarlu, C.H. Chen, J.S. Do, C.W. Lin, T.C. Chou, B.J. Hwang, Journal of Power Sources 146 (2005) 204–208.
[16] A.D. Robertson, H. Tukamoto, J.T.S. Irvine, Journal of the Electrochemical Society 146 (1999) 3958–3962.
[17] A.N. Jansen, A.J. Kahaian, K.D. Kepler, P.A. Nelson, K. Amine, D.W. Dees, D.R. Vissers, M.M. Thackeray, Journal of Power Sources 81 (1999) 902–905.
[18] X.L. Yao, S. Xie, C.H. Chen, Q.S. Wang, J.H. Sun, Y.L. Li, S.X. Lu, Electrochimica Acta 50 (2005) 4076–4081.
[19] W. Lu, I. Belharouak, J. Liu, K. Amine, Journal of Power Sources 174 (2007) 673–677.
[20] W. Lu, I. Belharouak, J. Liu, K. Amine, Journal of the Electrochemical Society 154 (2007) A114–A118.
[21] Y. Yu, J.L. Shui, C.H. Chen, Solid State Communications 135 (2005) 485–489.
[22] H. Kitaura, A. Hayashi, K. Tadanaga, M. Tatsumisago, Journal of the Electrochemical Society 156 (2009) A114–A119.
[23] M.E. Orazem, B. Tribollet, Electrochimica Acta 53 (2008) 7360–7366.

[24] R.D. Armstrong, Journal of Electroanalytical Chemistry 198 (1986) 177–180.
[25] S.K. Martha, O. Haik, V. Borgel, E. Zinigrad, I. Exnar, T. Drezen, J.H. Miners, D. Aurbach, Journal of the Electrochemical Society 158 (2011) A790–A797.
[26] S. Scharner, W. Weppner, P. Schmid-Beurmann, Journal of the Electrochemical Society 146 (1999) 857–861.
[27] N. Takami, K. Hoshina, H. Inagaki, Journal of the Electrochemical Society 158 (2011) A725–A730.
[28] E. Barsoukov, D.H. Kim, H.S. Lee, H. Lee, M. Yakovleva, Y. Gao, J.F. Engel, Solid State Ionics 161 (2003) 19–29.
[29] K. Dokko, M. Mohamedi, Y. Fujita, T. Itoh, M. Nishizawa, M. Umeda, I. Uchida, Journal of the Electrochemical Society 148 (2001) A422–A426.
[30] D. Andre, M. Meiler, K. Steiner, C. Wimmer, T. Soczka-Guth, D.U. Sauer, Journal of Power Sources 196 (2011) 5334–5341.
[31] D.M. Wu, Ionics 18 (2012) 559–564.
[32] P. Suresh, A.K. Shukla, N. Munichandraiah, Journal of Applied Electrochemistry 32 (2002) 267–273.
[33] H. Ishikawa, O. Mendoza, Y. Sone, M. Umeda, Journal of Power Sources 198 (2012) 236–242.
[34] R.B. Wright, C.G. Motloch, J.R. Belt, J.P. Christophersen, C.D. Ho, R.A. Richardson, I. Bloom, S.A. Jones, V.S. Battaglia, G.L. Henriksen, T. Unkelhaeuser, D. Ingersoll, H.L. Case, S.A. Rogers, R.A. Sutula, Journal of Power Sources 110 (2002) 445–470.
[35] R.B. Wright, J.P. Christophersen, C.G. Motloch, J.R. Belt, C.D. Ho, V.S. Battaglia, J.A. Barnes, T.Q. Duong, R.A. Sutula, Journal of Power Sources 119 (2003) 865–869.